Chemical Engineering Journal 440 (2022) 135869

Contents lists available at ScienceDirect

Chemical Engineering Journal

journal homepage: www.elsevier.com/locate/cej

Advanced MXene/shear stiffening composite-based sensor with high-performance electromagnetic interference shielding and anti-impacting Bi-protection properties for smart wearable device

Min Sang [a,b], Junshuo Zhang [a], Shuai Liu [a], Jianyu Zhou [a], Yu Wang [a], Huaxia Deng [a,*], Jun Li [b], Ji Li [b], Shouhu Xuan [a,*], Xinglong Gong [a,*]

[a] CAS Key Laboratory of Mechanical Behavior and Design of Materials, Department of Modern Mechanics, University of Science and Technology of China, Hefei, Anhui 230027, PR China
[b] Anhui Weiwei Rubber Parts Group Co. Ltd., Tongcheng, Anhui 231460, PR China

ARTICLE INFO

Keywords:
Smart wearable devices
Electromagnetic interference shielding
Anti-impact
Safe-guarding
Multiple sensing

ABSTRACT

Smart wearable devices with mechanical anti-impact property and electromagnetic interference shielding performance are highly required for providing comprehensive and effective protection for human beings under special conditions. Herein, a multifunctional SSE/MXene-NWF/SSE (SMS) sandwich composite with multiple sensing properties, electromagnetic interference shielding performance and anti-impacting ability was developed. By decorating conductive MXene onto the middle non-woven fabric (NWF), the as-fabricated SMS composite protects human from the harmful electromagnetic radiation with the shielding effectiveness up to 58 dB. The shear stiffening elastomer (SSE) whose storage modulus increases with the shear frequency displays typical shear stiffening effect, and thus confers SMS sandwich composite outstanding anti-impacting and safe-guarding properties which can dissipate nearly 97% impact energy. In addition, this SMS sandwich composite also meets the development needs of smart wearable devices, which can be comfortably attached onto human parts to monitor different human motions. Moreover, the intelligent alarm system and mechanical manipulator based on SMS sensor shows the promising application in wireless transmission and human–machine interaction. Finally, the designed SMS-based sensor array further displays its multi-perceptive characteristic under various stimuli as well as double-safeguarding abilities under impact and electromagnetic radiation. This work opens a new perspective for the development of multifunctional composite as smart wearable devices with anti-impacting and electromagnetic interference shielding properties for the comprehensive safeguarding of human beings.

1. Introduction

With the development of artificial intelligence, wearable electronic device has shown promising prospect in monitoring human body, human–machine interaction and wireless transmission fields [1–3]. Generally, this type of flexible electronic product has ideal flexibility, ductility and versatility, which can be perfectly attached to the skin as a wearable electronic sensor and maintain its function under complex external conditions. At the same time, the popularization of the wearable electronic sensor causes another problem, that is electromagnetic radiation, which has become an invisible killer of human health and cause huge impacts on human public health [4,5]. How to improve the electromagnetic interference shielding performance of the wearable electronic sensor, endowing the wearable electronic sensor with other protection functions is a major problem that needs to be solved in the era of artificial intelligence [6–10]. Studies show that the high conductivity of materials is the key factor determining the electromagnetic interference shielding performance [11–15]. In the past decade, many conductive materials such as carbon black [16], carbon nanotubes [17] and graphene [18] have been widely used in the field of electromagnetic shielding. However, compared with graphene, carbon black and carbon nanotubes have poor conductivity and high seepage threshold, while flake graphene has high conductivity, but its preparation steps are complicated and its yield is low. In recent years, two-dimensional transition metal carbides (MXenes) have shown great application potential in the field of high-performance electromagnetic shielding

* Corresponding authors.
E-mail addresses: hxdeng@ustc.edu.cn (H. Deng), xuansh@ustc.edu.cn (S. Xuan), gongxl@ustc.edu.cn (X. Gong).

https://doi.org/10.1016/j.cej.2022.135869
Received 19 January 2022; Received in revised form 27 February 2022; Accepted 15 March 2022
Available online 17 March 2022

materials due to their excellent metal-like conductivity, large specific surface area and typical two-dimensional sheet structure [19–23]. As a new two-dimensional material, MXenes have the advantages of high specific surface area and high conductivity (up to 14, 000 S/cm) similar to graphene, but also controllable nanolayer thickness and stable dispersion in water or organic solvents [24,25]. Gogotsi et al. fabricated a pure Ti_3C_2Tx film and the electromagnetic interference shielding value is up to 92 dB at the thickness of 45 μm. This is primarily attributed to the superior conductivity and unique lamellar structure of MXene nanosheets [26]. More importantly, MXene nanosheets can also be combined with polymer to construct a composite material with excellent electromagnetic interference shielding performance and other multi-functional properties.

Nowadays, the continuous development of science and technology has also brought new safety risks to human beings. The impact force from sports, car accidents and even war will not only pose a major threat to human life, but also it will damage the electromagnetic interference shielding performance of wearable equipment, making human beings face both impact force and electromagnetic radiation harms. In this case, it is an urgent need to develop smart wearable equipment with anti-impact and safeguarding properties against the external impact energy. As a smart material, shear stiffening material shows a wide application prospect in damping, vibration controlling, mechanical impact resistance and human safety protection [27–29]. The obvious characteristic of shear stiffening material is that its modulus increases rapidly when the external shear rate exceeds the critical shear rate [30,31], showing a change from a soft state to a solid state, and exhibiting strong ability to absorb the external impact energy. Very recently, it has been widely reported various intelligent wearable protective equipment based on shear stiffening material [32–35]. Xuan et al. developed a novel safeguarding tactile e-skins for monitoring human motion based on SSE-Ag NWs-PET hybrid structure. Due to the shear stiffening effect of SSE, e-skin exhibited excellent anti-impact and safeguarding properties which can effectively dissipate the external impact force [36]. Nevertheless, the wearable protective equipment based on SSE only possesses single mechanical protective performance, which cannot meet the requirements of modern wearable protective equipment designed for complex electronic environment. In addition, traditional electromagnetic interference shielding materials mainly focus on their ability of shielding radiation, and there are few studies on their mechanical strength and other functionalities. Therefore, how to develop advanced smart wearable sensor with high bi-protection performance against impact force and electromagnetic radiation, and ensure the personal safety has become a key problem to be solved in the field of human protection.

Sandwich structures, as an important innovative multifunctional structure, which possess the advantages of low density and high performance, have shown expansive application potential in sensing, electromagnetic interference shielding and energy absorption [37–39]. As EMI shielding materials, sandwich-structured composites possess the typical structures, which can concentrate the conductive filler in a certain layer to form a more effective conductive network and improve the conductivity of the conductive layer surface, thus improving the electromagnetic shielding performance of the material. On the other hand, the multilayer property of sandwich structure is also conducive to multiple reflection and absorption of electromagnetic waves, which further improves the electromagnetic shielding effect of the material. Gu et al [40] developed the sandwich-structured EMI shielding nanocomposite films with Fe_3O_4/PVA composite electro-spun nanofibers in the top and bottom layers and Ti_3C_2Tx/PVA composite electro-spun nanofibers in the middle layer, whose EMI shielding effectiveness (EMI SE) can reach 40 dB with the thickness of 75 μm. It was also found from the review that sandwich structures are viable candidates for energy absorption applications not only because of their light weight, but also due to the high-energy absorption capabilities [41]. More importantly, by forming the sandwich structure, the structure of different components can be combined, so as to give play to the performance advantages of different components, achieve complementarity and optimization, and thus endow the composite materials with high-performance and multi-functions.

In this work, a multifunctional SMS sandwich composite with sensing, anti-impact and electromagnetic interference shielding performance is developed by assembling SSE polymer as the top and bottom layers and highly conductive MXene-decorated non-woven fabric as the middle layer. The adoption of conductive MXene makes SMS sandwich composite possess remarkable electromagnetic interference shielding performance with the maximum shielding value of 58 dB. Since SSE polymer shows typical rate-dependent mechanical properties, the structural coupling of conductive MXene and SSE polymer further endows the SMS sandwich composite with excellent anti-impacting and safeguarding ability, thereby can absorb approximately 97% external impact energy. The fracture and disentanglement of molecular chains in SSE polymer are the main mechanism of energy absorption during the impact. In addition, SMS-based sensor as the smart wearable equipment shows sensing property, which can monitor various human body movements. The developed smart alarm system and controllable manipulator based on SMS sensor also shows its promising prospect in wireless transmission and human–machine interaction. The further designed SMS-based array displays multiple perception characteristics to various stimulus, indicating the multifunctional sensing property and safeguarding performance of SMS sandwich composite as the mart wearable device. Finally, its versatility confers SMS composite multiple functions and excellent application value, which is superior to other composites with single property. As an intelligent wearable device, the fabricated SMS composite provides a comprehensive and effective demand for human body.

2. Material and methods

2.1. Materials

Hydroxyl silicone oil, boric acid, octanoic acid and hydrochloric acid (HCl) were provided by Sinopharm Chemical Reagent Co., Ltd, Shanghai, China. The methyl vinyl silicone rubber (VMQ 110–2) was purchased from Shenzhen Muwei Technology Co., Ltd, China. Ti_3AlC_2 MAX phase with 400 mesh size were bought from 11 Technology Co., Ltd, Jilin, China. Lithium fluoride (LiF) was purchased from Aladdin Chemical Co., Ltd, Shanghai, China. Raw non-woven fabric (NWF) was commercially available product, China. All chemical reagents were used without further purification and ultrapure water was employed.

2.2. Synthesis of delaminated MXene nanosheets

Generally, 2 g of Ti_3AlC_2 phase was slowly added into the uniform solution with 40 mL of HCl (9 M) and 2 g of LiF in a Teflon beaker. After 24 h of reaction at 35 ℃, the Al layer was selectively etched from the Ti_3AlC_2 phase. To obtain multilayer MXene (m-MXene), the reaction product was washed repetitively with deionized water until its pH was approximately 6. After going through ultrasonic exfoliation in ice water for 2 h, the mixture was centrifuged for 1 h under 3500 rpm to collect the upper suspension with delaminated MXene nanosheets. Finally, the MXene colloidal suspensions with definite concentration were obtained.

2.3. Fabrication of SSE/M−NWF/SSE (SMS) sandwich composite

Briefly, hydroxyl silicone oil and boric acid with a weight ratio of 20:1 were stirred to form a homogeneous mixture. After heating at 160 ℃ for 90 min, a dash of octanoic acid was added. Then, the above mixture was stirred and followed heated at 160 ℃ for another 30 min. After cooling to the room temperature, a solid SSG polymer gel was obtained. Next, the SSG/PDMS composite was prepared by mixing SSG polymer, VMQ silicone rubber and benzoyl peroxide with a mass ratio of

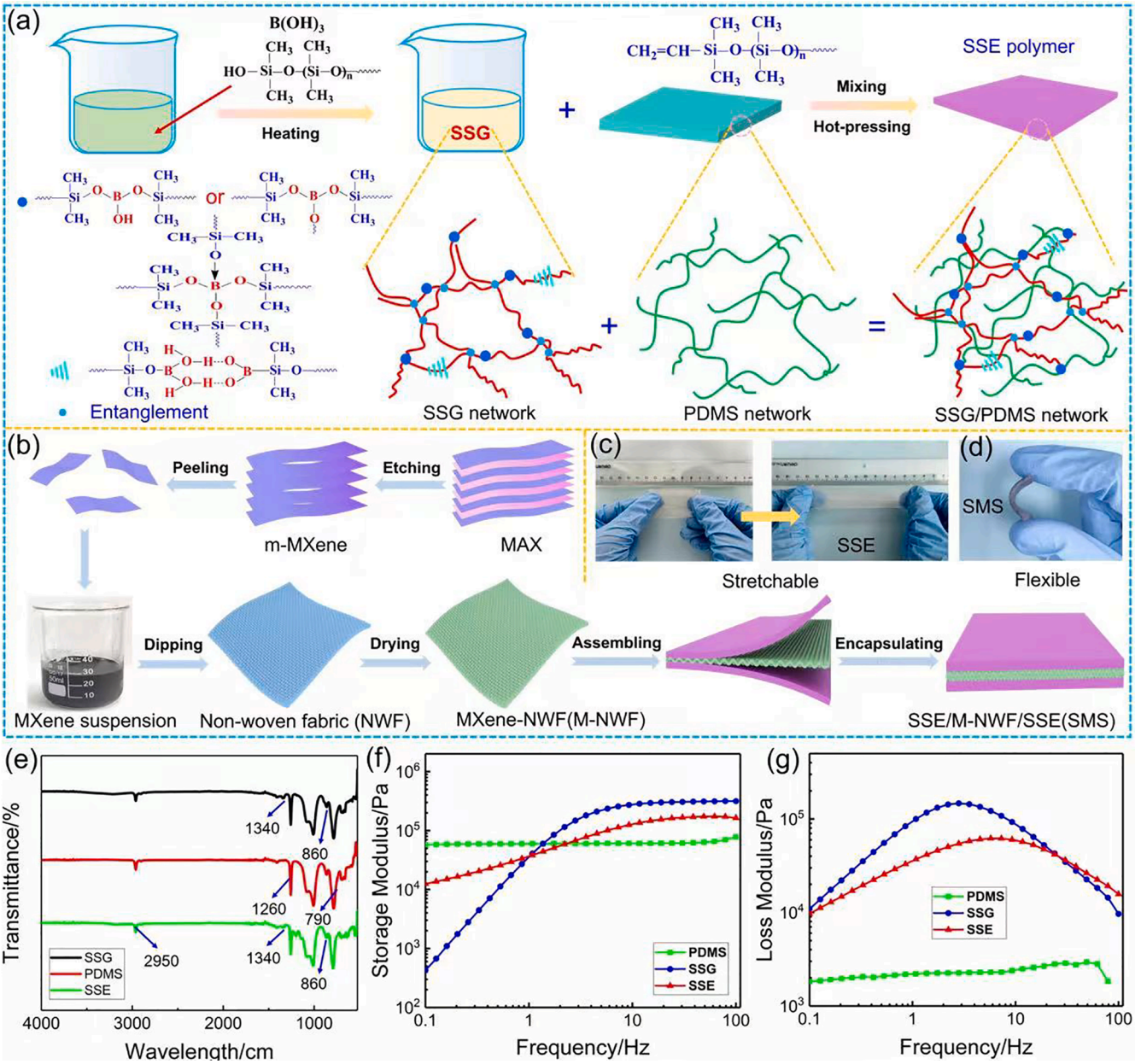

Fig. 1. (a) Schematic of fabrication process of SSE polymer. (b) Synthesis of MXene nanosheets and preparation of SMS sandwich composite. (c) The stretchability of SSE and (d) the flexibility of SMS sandwich composite. The (e) Fourier transform infrared (FT-IR) spectroscopy, (f) storage modulus and (g) loss modulus of SSG polymer, PDMS and SSE polymer.

7:3:0.4 using a two-roll miller. Then, the above SSG/PDMS composite was cured in a mould under 20 MPa at 100 ℃ for 15 min to acquire SSE polymer with the thickness of 0.8 mm. For the fabrication of MXene-decorated non-woven fabric (M−NWF), the pristine NWF was impregnated in the MXene solution with a concentration of 5 mg/mL and then dried in the oven at 55 °C for 10 min after each impregnation. Here, the different contents of MXene on the NWF were determined by controlling the impregnation numbers. After that, the obtained M−NWF was placed on the bottom SSE, and then the upper SSE was covered on the M−NWF. The size of the upper and lower SSE was slightly larger than the middle of M−NWF, thus the M−NWF could be successfully encapsulated in the middle because of the viscosity of SSE polymer.

2.4. Characterization

The Fourier transform infrared (FTIR) spectra of samples were acquired by using Nicolet 8700 equipment in ATR mode from 4000 to 400 cm^{-1}. The rheological properties of samples were measured by a commercial rheometer (Physica MCR 301, Anton Paar Co., Austria). Samples were molded into a cylinder shape with a thickness of 1.00 mm and a diameter of about 20 mm. The shear frequency varied from 0.1 to 100 Hz and the strain was set at 0.1%. The testing temperature was set as 25 ℃. The surface and cross-sectional morphologies of samples were characterized by scanning electron microscopy (SEM, Sirion 200, accelerating voltage of 10 kV) equipped with an energy-dispersive spectroscopy (EDS, accelerating voltage of 15 kV) system. The mechanical properties of SSE and conductive non-woven fabric were tested by the Materials Test System (MTS) and the optical measure system equipped with a CCD camera. During the test, the tensile rate was set to one thousandth of the effective length of the sample. The standard four-point contact method on a four-point probe (FT-340, Ningbo rooko instrument Co., Ltd., China) was used to test the electrical conductivity. A

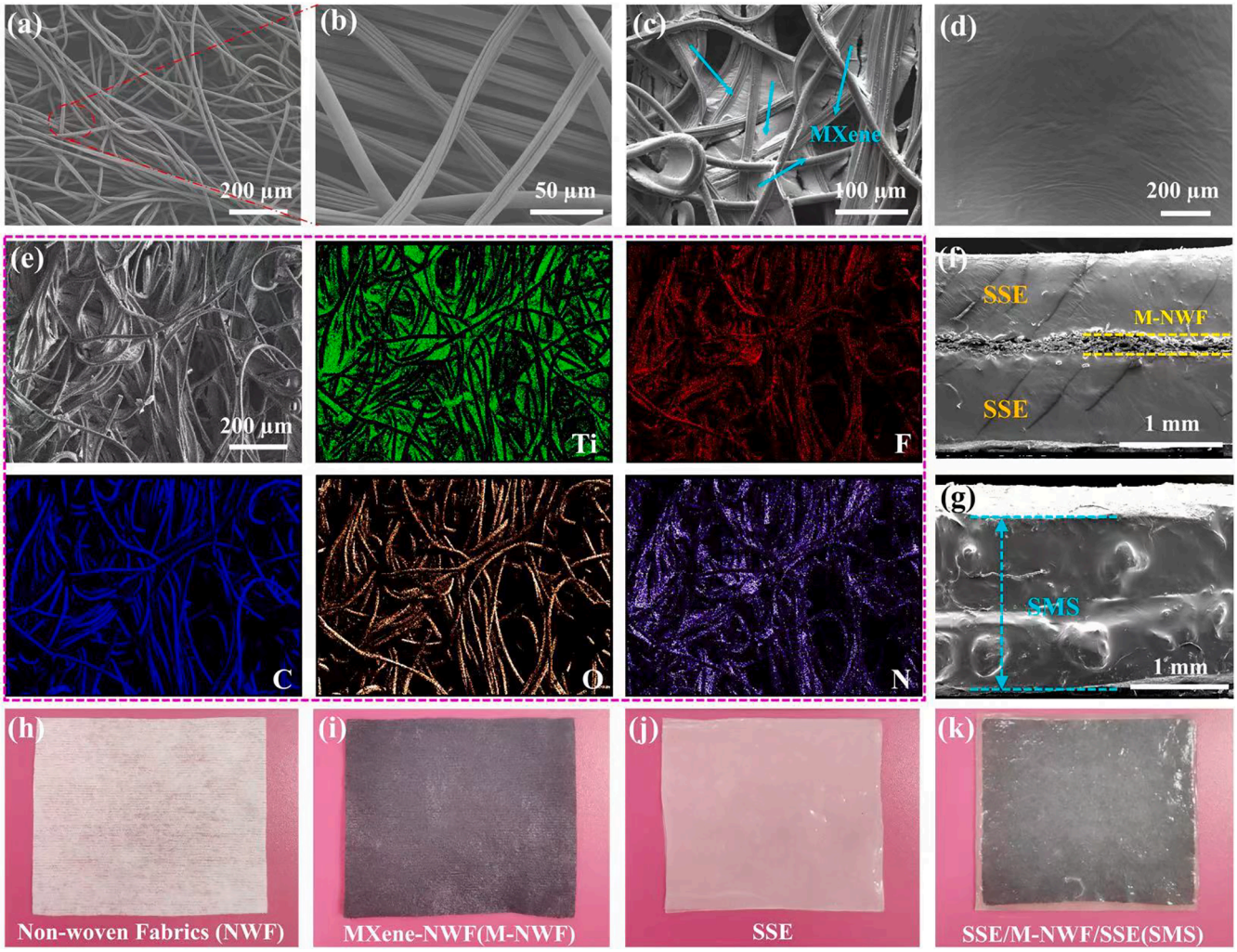

Fig. 2. The surface morphologies of the (a, b) raw NWF, (c) M−NWF and (d) SSE. (e) The elemental mapping images of M−NWF. The cross-sectional morphologies of (f) fractured SMS sandwich composite and (g) encapsulated SMS sandwich composite. The digital images of (h) non-woven fabric (NWF), (i) MXene-decorated NWF (M−NWF), (j) SSE and (k) SMS sandwich composite.

commercial vector network analyzer (AV3672, China electronics technology instruments Co., Ltd) was utilized to evaluate the electromagnetic interference shielding performance of samples in the 8–12 GHz region (X-Band). Samples were cut into the size of 22.9 × 10.2 mm^2 for the test. During the test, the specimen was installed in a copper clamp and then connected between two wave-guide flanges. The drop hammer test device with the force sensor and acceleration sensor was used to explore the energy dissipation property of samples. During the test, samples were cut into the size of 2 × 3 × 0.4 cm^3 and the drop hammer fell from different heights to impact the sample. The electrical signals under the external stimuli were recorded by a ModuLab material test system (MTS) (Solartron analytical, AMETEK advanced measurement technology, Inc., United Kingdom). The thickness of SSE layer and M−NWF layer were measured by a digital micrometer (Sanliang Corporation, 0–25 mm).

3. Results and discussion

3.1. Fabrication and property of SSE polymer and SMS sandwich composite

The fabrication process of SMS sandwich composite shown in Fig. 1 consists of three main steps: fabrication of SSE polymer, fabrication of MXene-decorated non-woven fabric and assembly of these elements. As shown in Fig. 1a, shear stiffening gel (SSG) was acquired through chemical polymerization by mixing hydroxyl silicone oil and boric acid at 160 ℃, where some physical cross-linking (hydrogen bonds, dative bonds between B and O elements in the Si-O groups, and topological entanglements) can be formed during this process [42,43]. After that, SSE polymer was further prepared through hot-pressing at 100 ℃ under 20 MPa by blending SSG polymer and PDMS polymer to form SSG/PDMS double network. The fabrication of MXene-decorated non-woven fabric (M−NWF) was achieved via a simple dipping and drying method. By etching Al layer from MAX phase and further exfoliating multilayer MXene, the delaminated MXene suspension was obtained. To confirm the successful synthesis of MXene nanosheets, XRD and TEM characterizations are presented in Figure S1. The disappearance of strong peak (1 0 4) at 39° of MXene indicates that Al layer is completely removed from Ti_3AlC_2 (Figure S1a). The TEM image shows the typical lamellar structure of MXene nanosheets with the size of several hundred nanometers (Figure S1b). The final prepared MXene solution appears dark black.

To fabricate the Mxene-NWF, the pristine non-woven fabric (NWF) was immersed into the above MXene suspension several times and dried in the oven at 50 ℃ to gain M−NWF with different MXene contents. In this work, the main components of the non-woven fabric (NWF) used are viscose fiber and polyester, which contains a large number of ester groups. These ester groups can interact with the –OH, -O, and -F

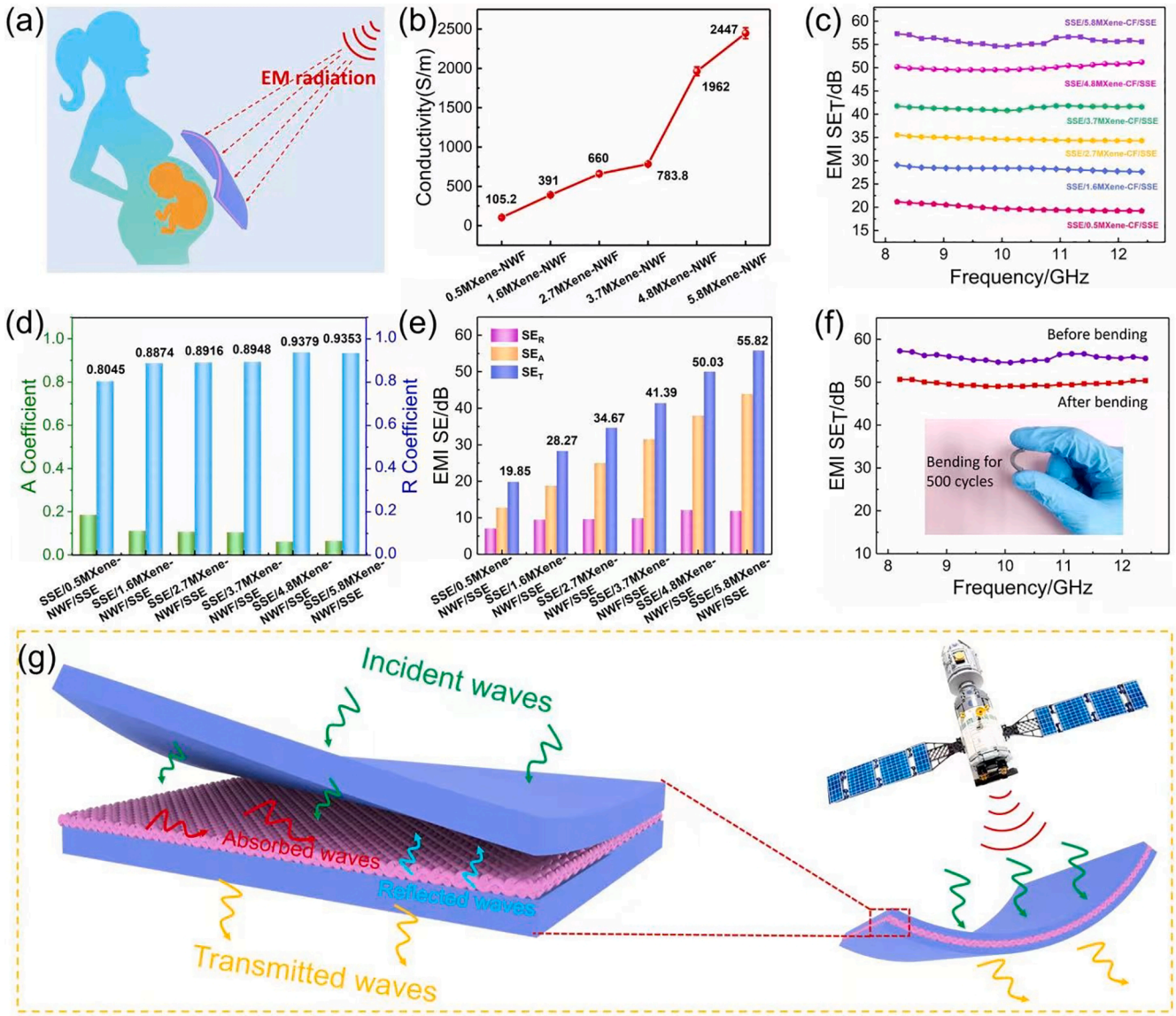

Fig. 3. (a) The schematic diagram of SMS sandwich composite against electromagnetic radiation for protecting the pregnant woman. (b) The electrical conductivity of MXene-decorated NWF (M−NWF) with different MXene contents. (c) Electromagnetic interference shielding efficiency, (d) R and A coefficients, (e) average EMI SE_T, SE_A and SE_R values of SMS sandwich composite with different MXene contents. (f) The electromagnetic interference shielding performance of SMS sandwich composite before and after cyclic bending.

functional groups on the surface of MXene, thus improve the interfacial force between MXene nanosheet and NWF, and MXene can be successfully attached to the NWF. In order to prove the interaction between MXene nanosheets and NWF, the NWF impregnated with MXene was put in deionized water for ultrasonic 24 h. It can be found that MXene on the NWF hardly fell off, indicating that MXene has good adhesion on the NWF (Figure S2). Ultimately, the M−NWF was encapsulated in the middle layer by the upper and lower SSE to manufacture SSE/M−NWF/SSE (SMS) sandwich composite (Fig. 1b). During the assemble process, only the preparation of SSE requires hot pressing at 100 ℃ under 20 MPa by blending SSG polymer and PDMS polymer, while the M−NWF in the middle will not undergo the process of hot pressing, so the oxidation of MXene in the fabrication process can be avoided. In addition, the viscosity and self-healing property of SSE polymer can promote the close connection between the interfaces of sandwich structure and successfully wrapped the M−NWF in the middle layer without separation, thus the contact between MXene and air can be avoided, and avoide the oxidation of MXene.

Here, in the novel SSG/PDMS double network, the strong covalent networks in PDMS endow SSE with toughness and elasticity (Fig. 1c), while the supramolecular networks in SSG confer shear stiffening effect and self-healing property. Fig. 1d shows the flexibility of the fabricated SMS sandwich composite which can be bent freely. From FTIR spectroscopy of SSG, the characteristic band at 1340 cm^{-1} and 860 cm^{-1} correspond to the Si-O-B bonds and B-OH out-of-plane bending, indicating the successful cross linking of boric acid molecule with hydroxyl silicone oil polymer chain. However, for PDMS, the characteristic band at 1340 cm^{-1} and 860 cm^{-1} correspond to the Si-O-B bonds and B-OH out-of-plane bending are absent. After introducing PDMS into SSG, the hybrid polymer SSE also inherits Si-O-B bonds, thus shows similar results with SSG polymer. Besides, the characteristic band at 2930 cm^{-1} refers to the $–CH_3$ group, which exists in SSG, PDMS and SSE polymer (Fig. 1e). As shown in Fig. 1f and g, the rheological tests were employed to explore the shear rate-dependent properties of SSG polymer and SSE polymer. For PDMS polymer, the storage modulus and loss modulus both are independent of frequency, which indicates that PDMS has no shear stiffening effect. On the contrary, the initial storage modulus of SSG polymer at 0.1 Hz is 427 Pa while it increases sharply with the shear

frequency increases and the maximum storage modulus is up to 0.32 MPa (100 Hz), demonstrating the typical shear stiffening effect. Inheriting this characteristic from SSG, the SSE polymer also possesses remarkable shear stiffening property whose storage modulus increases with the increase of shear frequency (12500 Pa increases to 0.16 MPa) (Fig. 1f). Fig. 1g presents the rate-dependent property of loss modulus, which states the energy dissipation performance of SSG and SSE polymer. In this work, SSG was synthesized by the reaction of hydroxyl silicone oil and $B(OH)_3$, whose possible molecular formula was shown in Fig. 1a. When the supplied $B(OH)_3$ are introduced into hydroxyl silicone oil, electron-rich O atoms would share electrons with electron-deficient B atoms to form "B-O coordination bonds". The formation of "B-O coordination bonds" is the root of the shear stiffening properties of SSG. This "B-O coordination bond" is transient, dynamically variable and more vulnerable than covalent bond. When the external shear frequency increases, the relaxation time of the"B-O coordination bonds" is higher than the external frequency, which could not catch up with the change of the external stimulus. As a result, many "B-O coordination bond" may attract polymer chains and block the movement of other molecular chains. In this case, a large number of"B-O coordination bond" in a short time can severely impede the movement of the internal molecular chains during the shear process, which make SSG exhibit solid property. Therefore, SSG polymer shows shear stiffening property owing to the"B-O coordination bonds" supplied by $B(OH)_3$.

3.2. Characterization of SSE polymer and SMS sandwich composite

Scanning electron microscopy (SEM) was conducted to characterize the microstructure (Fig. 2). The pristine non-woven fabric (NWF) shows irregular network structures formed by smooth fiber bundles (Fig. 2a). A lot of voids exist in the network, which provides abundant sites for the adhesion of flaky MXene (Fig. 2b). After dipping NWF into MXene colloidal suspensions, lamellate MXene obviously fills the void of NWF (Fig. 2c). Fig. 2d demonstrates the micro-wrinkled surface morphology of SSE polymer, which indicates its elasticity and flexibility. Besides, the elemental mapping images of M−NWF depict the spatial distribution of Ti, F, C, O and N elements, which further testifies the successful incorporation of conductive MXene nanosheets (Fig. 2e). The cross-sectional morphologies of fractured SMS sandwich composite and encapsulated SMS sandwich composite were presented in Fig. 2f and g, respectively. It can be seen that the three-layered structure is clearly visible from the fractured cross-sectional image, where the middle conductive MXene-decorated non-woven fabric (M−NWF) is closely connected with the upper and lower layers of SSE. From encapsulated cross-sectional image, there is no obvious gap between the three layers, which indicates that the upper and lower layers of SSE can well package the M−NWF in the middle layer. Thus, it is confirmed that the three-layered composites can achieve better integration due to the viscosity and self-healing property of SSE polymer. In addition, the digital images of raw NWF, M−NWF, SSE and SMS sandwich composite were exhibited in Fig. 2h-k. For SSE polymer, its appearance is colorless and has a certain transparency (Fig. 2j). Therefore, the black M−NWF in the middle can be clearly seen after wrapping the M−NWF with transparent SSE (Fig. 2k).

3.3. The electromagnetic interference (EMI) shielding ability of SMS sandwich composite

Electromagnetic waves emitted by electronic devices can cause adverse effects on the fetus in pregnant women. The SMS sandwich composite filled with continuously conductive pathways of MXene flakes in the non-woven fabric (NWF) is expected to possess superior EMI shielding performance, thus protects pregnant women from the harm of electromagnetic waves (Fig. 3a). Here, EMI shielding efficiency (EMI SE), R and A coefficient were calculated from the S parameters measured by the vector network analyzer on the basis of the following equations [44–46]:

$$R = |S_{11}|^2 \tag{1}$$

$$A = 1 - |S_{11}|^2 - |S_{21}|^2 \tag{2}$$

$$SE_R = -10lg\left(1 - |S_{11}|^2\right) \tag{3}$$

$$SE_A = -10lg\left(\frac{|S_{21}|^2}{1 - |S_{11}|^2}\right) \tag{4}$$

$$EMI\ SE = SE_A + SE_R \tag{5}$$

As shown in Fig. 3b, SMS sandwich composite shows the increased electrical conductivity with higher MXene content. The surface conductivity of 5.8MXene-NWF can be as high as 2447 S/m, which was attributed to the highly efficient MXene conductive networks on the non-woven fabric. High electrical conductivity is a precondition for the effective EMI shielding ability of SMS sandwich composite. Thus, with the MXene content increased from 0.5 to 5.8 mg/cm^2, the EMI SE_T value of SMS sandwich composite shows a significant rising trend from 19.85 to 55.82 dB in the X band (Fig. 3c).

To analyse the EMI shielding mechanism of SMS sandwich composite, the absorption coefficient (A) and reflection coefficient (R) were calculated. As shown in Fig. 3d, R value is much higher than A value regardless of the MXene content, illustrating that SMS sandwich composite is highly reflective material. In this work, the fabricated SMS composite is composed of three layers, including the upper and lower layers of non-conductive SSE polymer and a conductive MXene-NWF in the middle. Since the upper and lower layers of non-conductive SSE polymer are transparent to electromagnetic waves, the incident electromagnetic waves would interact with the conductive MXene-NWF in the middle. Owing to the high electrical conductivity of MXene nanosheets, significant impedance mismatch occurs at the MXene and air interface, thus most of the electromagnetic waves are reflected. Although SMS sandwich composite possesses layered structure, due to the impedance matching between SSE polymer and air interface, electromagnetic waves reflected from the conductive MXene-NWF in the middle will not be reflected again when passing through the SSE layer, but directly go through the SSE polymer and enters the air, thus SMS sandwich composite is mainly highly reflective materials. Therefore, the primary EMI shielding mechanism of SMS sandwich composite is reflection loss, and only a small part of incident electromagnetic waves can enter into the composite to be absorbed. Additionally, the total values of R and A of SMS sandwich composite are approximately 100%, demonstrating that most of the incident electromagnetic waves have been shielded. Moreover, the contribution of SE_A to the overall SE_T is predominate, also indicating the highly effective attenuation of entered electromagnetic waves within the SMS sandwich composite (Fig. 3e).

As a wearable EMI shielding material, flexibility and robustness are necessary properties during the practical application. Under the cyclic external deformation or impacting, it is important whether the composite can maintain the high EMI shielding ability. As exhibited in Fig. 3f, after 500 continuous bending deformation, SMS sandwich composite still keep a high electromagnetic interference shielding capability with the EMI SE value of 51 dB. In order to explore the electromagnetic shielding performance after impacting, we tested the conductivity and electromagnetic interference shielding performance of SSE/5.8MXene-NWF/SSE sample after impacting at 10 cm and 20 cm drop heights. For the unbroken samples after impacting test, the electromagnetic interference shielding values after impacting can reach 48 dB and 43 dB under 10 cm and 20 cm drop heights, respectively (Figure S3a), which is still highly greater than the commercial requirements (20 dB), indicating that the SMS composite still possesses considerable electromagnetic interference shielding performance after impacting. Besides, the SMS composite also possesses high conductivity after impacting (Figure S3b), thus guarantees the outstanding

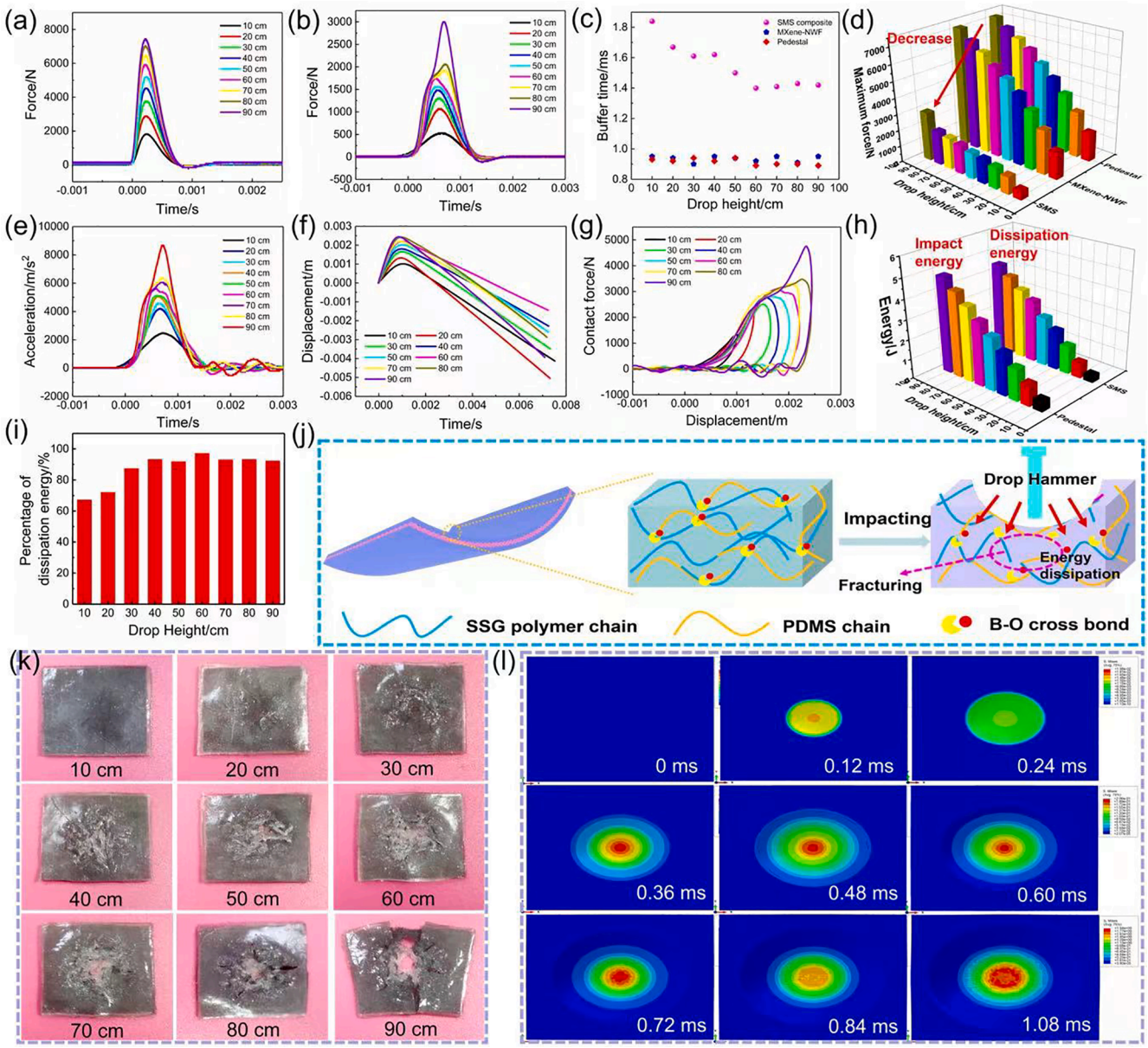

Fig. 4. Typical force–time curves of (a) pedestal and (b) SMS sandwich composite from different drop heights of 10–90 cm, respectively. The comparison of (c) buffer time and (d) force values between pedestal and SMS sandwich composite at different drop heights (10–90 cm). (e) The acceleration-time curve, (f) displacement–time curve and (g) force–displacement curve of SMS sandwich composite at different drop heights (10–90 cm). (h) Impact energy dissipation behavior and (i) percentage of dissipation energy for SMS sandwich composite at different drop heights (10–90 cm). (j) The mechanism of the energy dissipation behavior for SMS sandwich composite. (k) The practical pictures of the SMS sandwich composite damaged by drop hammer impact. (l) Finite elements simulation results of stress distribution of SMS sandwich composite at different drop heights (10–90 cm).

electromagnetic interference shielding property. Moreover, the sandwich structure makes the SSE polymer on both sides of the SMS composite and the MXene-decorated NWF in the middle of the SMS composite, preventing the MXene nanosheets from oxidation due to contact with O_2 in the air. To prove the oxidation resistance, we conducted XRD test on the MXene-decorated NWF in the middle of the SMS composite. According to XRD result (Figure S4), the peak absence of TiO_2 indicates that MXene was not oxidized during the test, thus further guaranteeing the stability and durability of EMI shielding ability of the SMS sandwich structure [40]. Finally, the reflection loss for the incident electromagnetic waves and effective attenuation for the entered electromagnetic waves are primarily ascribed to the ideal conductive network of MXene nanosheets and sandwiched structure of SMS composite (Fig. 3g). Here, the EMI shielding performance of other previously reported composites are also consulted in Table S1 [39,40,47–51]. It is found that the fabricated SMS composite as EMI shielding material shows an excellent EMI shielding ability and the flexibility guarantees its stability and durability in the practical application.

3.4. The anti-impacting, energy dissipation performance and finite elements analysis simulation of SMS sandwich composite

Due to the rate-dependent shear stiffening effect of SSE polymer, the anti-impacting and energy dissipation performance of SMS sandwich composite were systematically explored. A drop hammer device equipped with force sensor, acceleration sensor, charge amplifier and oscilloscope was employed on the SMS sandwich composite (Figure S5). The weight of drop hammer is 0.55 kg with the falling height varying from 10 to 90 cm to impact the sample perpendicularly. During the impact, the SMS sandwich composite was placed on the force sensor, which is

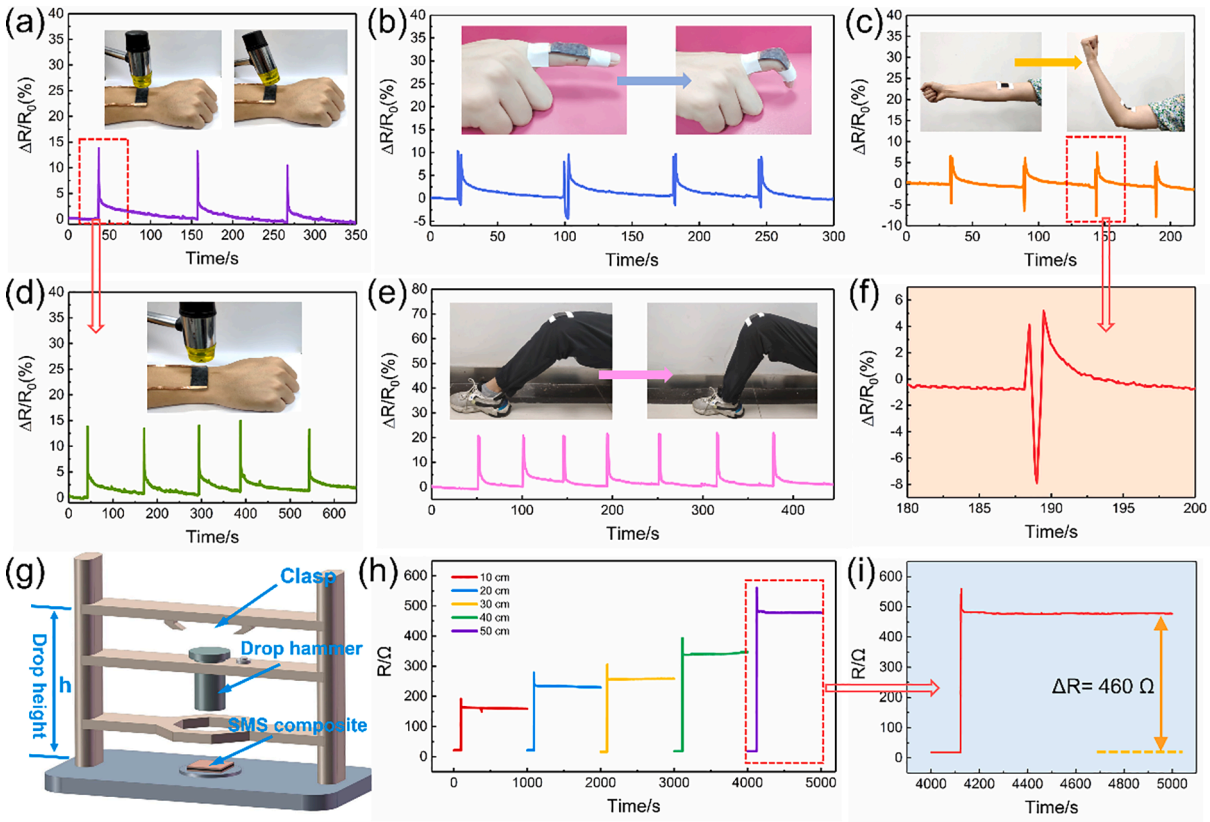

Fig. 5. The electrical signals of SMS sandwich composite under different external stimuli, such as (a, d) small hammer beating, (b) finger bending, (c, f) arm bending, (e) knee bending and (h, i) drop hammer beating. (g) Schematic diagram of drop hammer device.

further fixed on the metal pedestal. Fig. 4a and b shows the typical force–time curves of pedestal and SMS sandwich composite from different drop heights of 10–90 cm during the impact process. Once the drop hammer contacts the pedestal or SMS sandwich composite, the impact force detected by the force sensor quickly increases to a maximum value and then declines to approximately zero in a short time. The higher the drop height, the greater the maximum impact force. Compared with the pedestal, the maximum impact force of the conductive MXene-NWF in the middle has no attenuation (Figure S6a), indicating that the anti-impacting and energy dissipation performance depends on the upper and lower SSE polymer layers. Thus, the maximum impact forces of SMS sandwich composite are significantly reduced and the buffer time is significantly prolonged under 10–90 cm drop height, indicating the apparent impact resistance and energy absorption properties of SMS sandwich composite (Fig. 4c and d). In order to explore the influence of SSE component on the anti-impacting performance, Figure S7a-b show the impact force of SSE polymer with different thicknesses of 0.8 mm and 1.8 mm under different drop heights. It can be seen that the larger the thickness of SSE polymer is, the smaller the force is, indicating the better anti-impact performance (Figure S7c).

To further quantitatively analyze the energy dissipation capacity of SMS sandwich composite, the acceleration of the hammer was recorded by acceleration sensor under 10–90 cm drop height so as to calculate the dissipated energy. According to the acceleration-time curve (Fig. 4e), the impact velocity, displacement and contact force of the hammer when contacting the SMS sandwich composite were calculated with following equations [52]:

$$V_0 = \sqrt{2gh_o} \tag{6}$$

$$V(t) = V_0 - \int_0^t a(t)dt \tag{7}$$

$$X(t) = \int_0^t v(t)dt \tag{8}$$

$$F(t) = ma(t) \tag{9}$$

where V_0 is the initial velocity of the drop hammer, g is the acceleration of gravity, h_0 is the drop height of the hammer, m is the weight of drop hammer, V(t) is velocity of the hammer varying with time in the impact progress, a(t) is acceleration of the hammer varying with time, X(t) and F(t) is the downwards vertical displacement and contact force of the hammer when contacting the SMS sandwich composite, respectively. With different drop height varying from 10 to 90 cm, the impact energy (E_0) can be calculated by the following equation:

$$E_0 = mgh_0 \tag{10}$$

Thus, the impact energies of the drop hammer applying on the SMS sandwich composite are 0.539 J, 1.078 J, 1.617 J, 2.156 J, 2.695 J, 3.234 J, 3.773 J, 4.312 J and 4.851 J, respectively.

Fig. 4f exhibits displacement–time curves of SMS sandwich composite at different drop heights, which shows that the contact displacement increases with the drop height. To figure out the dissipated energy of SMS sandwich composite, the contact force–displacement curves were plotted and shown in Fig. 4g. Thus, the integral area of the contact force–displacement curve is the dissipated energy at different drop heights. As shown in Fig. 4g, the dissipated energies of SMS sandwich composite are remarkably close to the impact energy of the hammer, which proves that SMS sandwich composite possesses unprecedented ability to dissipate the impact energy and the maximum percentage of dissipated energy can up to 97% at 60 cm drop height (Fig. 4h). Since the MXene-decorated non-woven fabric (M−NWF) has no anti-impacting property (Fig. 4d), the energy dissipation performance of SMS sandwich composite was attributed to the addition of SSE

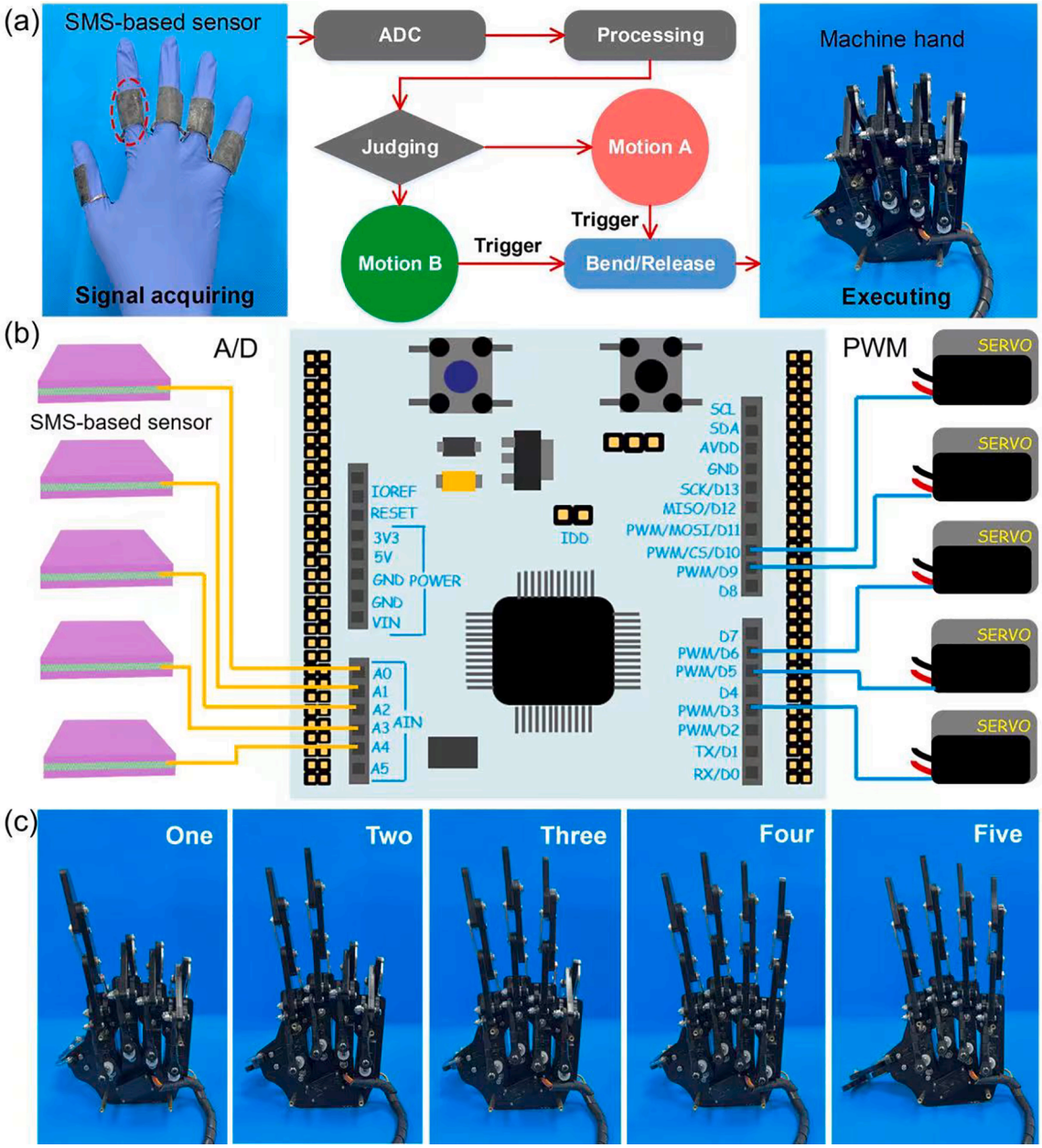

Fig. 6. (a) Schematic diagram showing the interaction of human hand and machine hand based on SMS-sensor. (b) The controlling circuit of the machine hand controlling system consist of five signal acquistion circuit, a micro control unit and five servos. (c) Photographs of controlling the machine hand by displaying the geatures from one "one" to " five".

polymer. Fig. 4i demonstrates the mechanism of the energy dissipation behavior for SMS sandwich composite. A large number of B-O crosslink bonds exist in the internal network of the SSE polymer, which are dynamic and reversible (Fig. 1a). Once the SMS sandwich composite was impacted by the hammer, the B-O crosslink bonds interact with each other to lock the entangled molecular chains. Finally, the SSE polymer absorbs and dissipates most of the impact energy through the fracturing and disentanglement of the entangled molecular chains. The unique energy dissipation property of SSE polymer makes SMS sandwich composite show promise application in the field of human body protection.

In the drop hammer tests, the stress distribution on the SMS sandwich composite were not able to be clearly shown. Thus, the finite element analysis (FEA) simulations were used to explore the stress distribution during the impact process. Here, the tensile tests were conducted to obtain the Poisson's ration of SSE polymer (0.41) and M−NWF (0.28), which was further used for the FEA simulation (Figure S8). As exhibited in Fig. 4l, it takes 1.08 ms to complete the entire impact process, and each image is separated by 0.12 ms. When the drop hammer contacts the SMS sandwich composite, stress waves spread out at the same speed from the central area where the drop hammer touches. Since the drop hammer has a certain falling speed (Figure S5a), with the passage of time, the displacement of the drop hammer contact sample increases (Fig. 4f), thus the stress applied on the SMS sandwich composite material increases at the same time. The closer to the central contact region, the more concentrated the stress on the SMS sandwich composite. Thus, the stress applied on the SMS sandwich composite is not uniform, the central region suffered more concentrated stress will be damage more seriously. Consistent with the results of finite element simulation, the practical pictures of the SMS sandwich composite under the impact in Fig. 4k also states that the damaged area is mainly concentrated in the contacted area by the drop hammer. Consequently, the destruction leads to the fracture of a large number of molecular

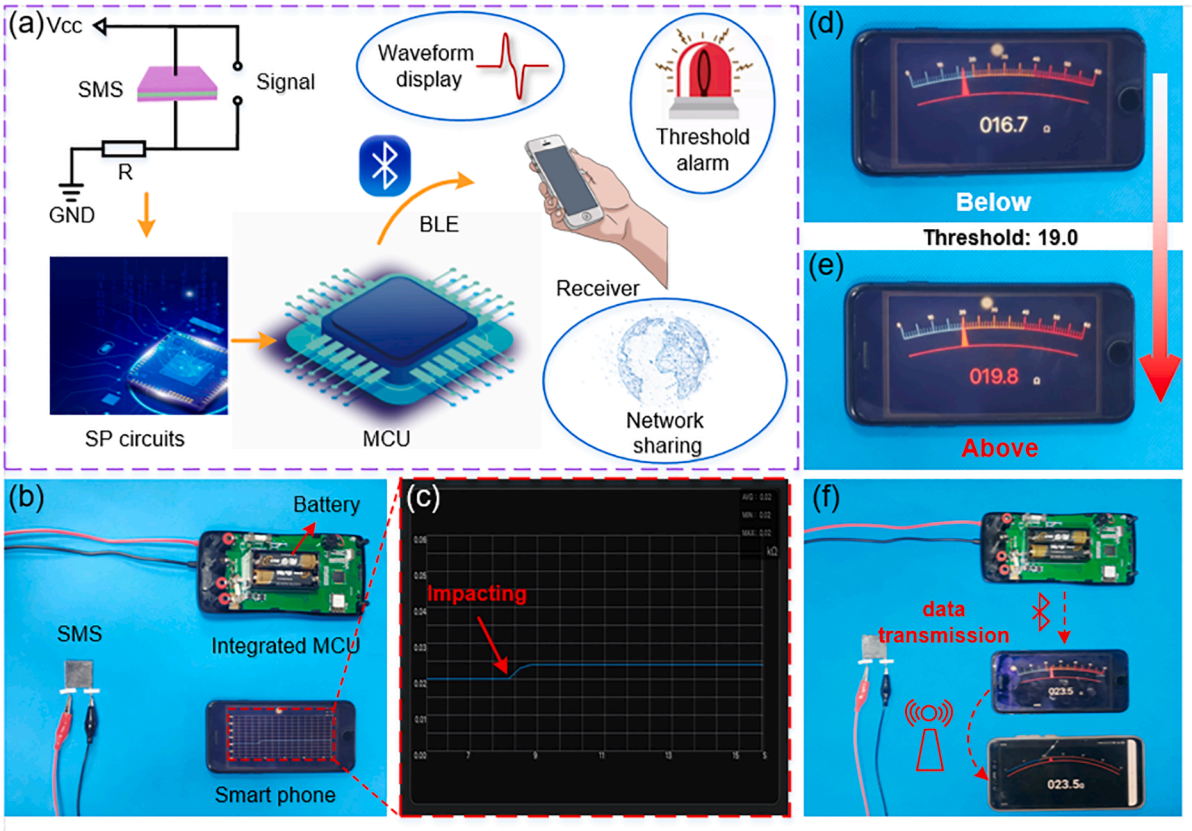

Fig. 7. (a) Schematic diagram of the wireless sensing system based on SMS sensor and application prospect of the wireless Bluetooth system for waveform displaying, threshold alarming and network sharing. (b) The experimental device diagram of SMS-based wireless sensing system includes SMS sensor, integrated MCU and a smart phone. (c) The sensing data collected by the smart phone under impacting. Real-time resistance value of SMS sensor in (d) initial state and (e) impact state. (f) The data transmission of SMS-based wireless sensing system.

chains in the SSE polymer, which dissipates a large amount of the impact energy.

3.5. The human body monitoring and impact-sensing property of SMS-based sensor

Owing to the superior electrical conductivity of MXene network, the SMS sandwich composite shows great promise in human body monitoring as the wearable sensor. Thus, the SMS-based sensor was fabricated and conformably attached to different position of human body to monitor the complicated body movements in real time. As shown in Fig. 5a, the SMS-based sensor can sensitively perceive the external tapping force on the skin by integrating it on the wrist. Moreover, the relative resistance values exhibited great stability and cyclicity at the same beating force, indicating the accurate sensing ability to external stimuli (Fig. 5d). The SMS-based sensor is also sensitive enough to distinguish the bending behavior of the forefinger, arm and knee, showing different relative resistance magnitude due to the various deformation caused by the bending movement (Fig. 5b, c, e and f). The stability of relative resistance further confirms the reliability of sensing property. Other than these mild motion by human body, the SMS-based sensor can also be used to sense huge impacting force generated by the drop hammer. Fig. 5g shows the schematic diagram of drop hammer device, where a 0.55 kg of drop hammer is released freely from different heights, touching the sensor and creating impacting force on the sensor. In the initial state, the resistance of sensor maintains about 10 Ω. When the sensor is impacted by the drop hammer, the resistance increases sharply to a maximum value. After the drop hammer is removed, the resistance is eventually maintained at a balance value (Fig. 5h, i). Since the drop hammer will cause certain damage to the conductive network of the sensor during the impacting process, the resistance of the sensor will be improved after impacting (Fig. 5i). The greater impact force leads to larger change of resistance value (ΔR), demonstrating the sensitivity of sensor to detect different impacting force. In light of these results, the fabricated SMS-based sensor can be used not only to monitor slight human movements, but also to detect drastic external impact force, showing the promise prospect for wearable devices detecting external stimuli in full range.

3.6. The intelligent controlling system of machine hand based on SMS wearable sensor towards human–machine interaction

From the above results, the as-developed SMS wearable sensor possesses ideal ability to monitor a range of human motions (Fig. 5). The electrical signals obtained from joint movements will show prospective potential in artificial intelligence and human–machine interactions. Thus, an intelligent controlling of machine hand based on SMS wearable sensor was successfully demonstrated (Fig. 6). The human–machine system mainly consists of signal acquisition process and robot execution process (Fig. 6a). Fig. 6b further displays the detailed working principle of intelligent controlling system of machine hand based on SMS wearable sensor. During the test, one end of the SMS-based sensor is connected to the power supply and the other end is connected to the circuit. When the SMS-based sensor attached on the human finger deforms, the resistance of the sensor will obviously change, leading to the change of current. Then, the current change is transformed into the voltage change by the acquisition circuit, which is further transmitted to the microprocessor as the input signal. Finally, the microprocess receives the pulse width modulation (PWM) and controls the rotation of the corresponding servo motor, making the bending/releasing of the machine

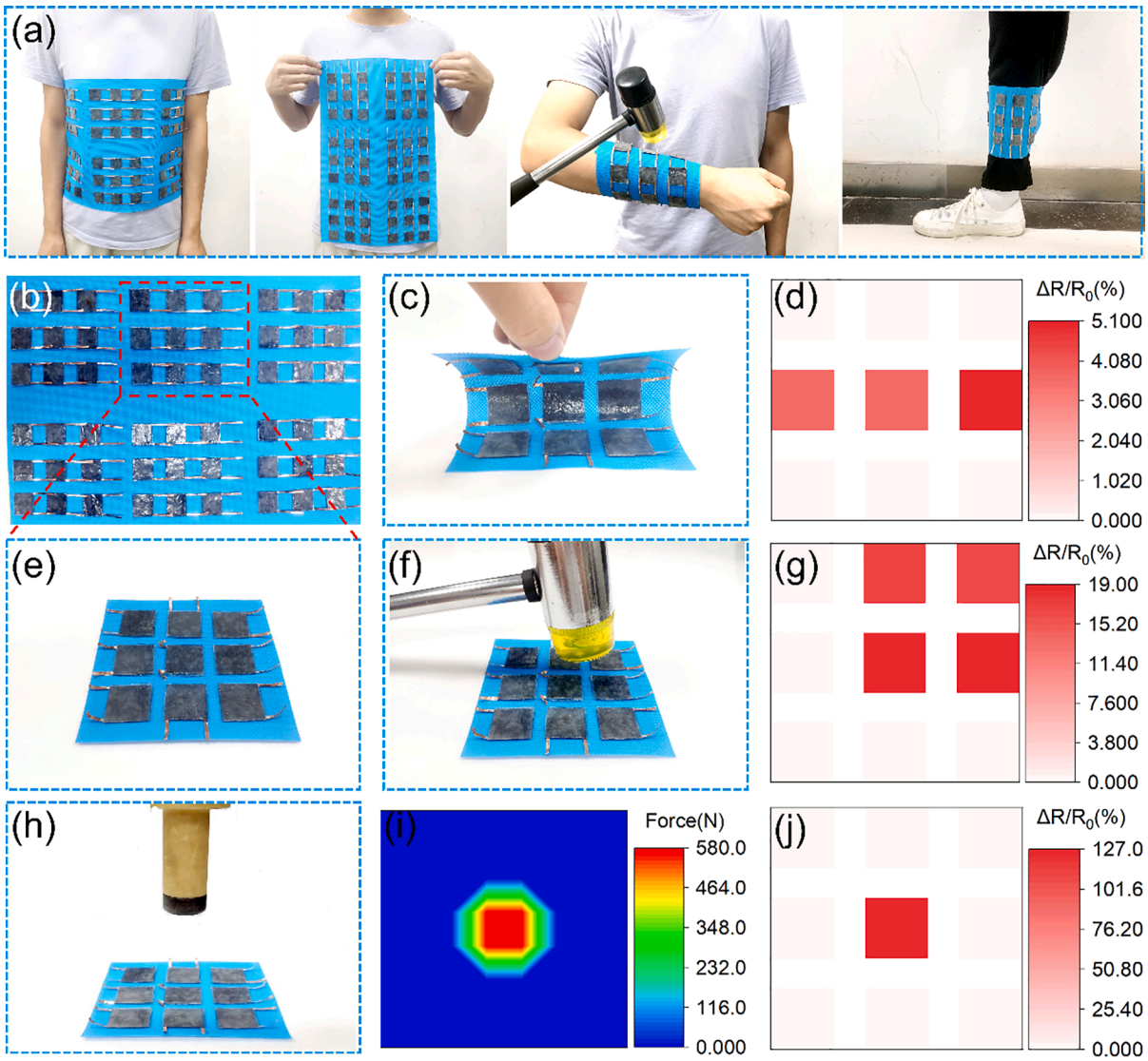

Fig. 8. (a) The anti-impact and safeguarding performance of SMS-based pads to safeguard human body. (b) The picture of SMS-based pads with 6 of 3 × 3 arrays. (e) The photograph of the 3 × 3 sensor array. Recognition of the pressure distribution of 3 × 3 sensor array under (c-d) bending, (f-g) hammer beating and (h-j) dynamic drop hammer impacting.

hand. Fig. 6c shows the successful controlling of machine hand by displaying the gestures from "one" to "five", indicating that the machine hand can response to the external stimuli generated by the human movements accurately, realizing the interaction of human and machine. Besides, Video S1 demonstrates the real-time and quick controlling process of machine hand.

3.7. The SMS-based wireless sensing system as a warning device towards safety protection

Recently, wireless Bluetooth sensing system has showed a broad application prospect in waveform displaying, threshold alarming and network sharing [53–55]. With the excellent sensing advantage of SMS sensor, a smart wireless sensing system as a warning device towards safety protection was developed (Fig. 7a). The SMS-based wireless sensing system consists of signal processing (SP) circuits, a micro control unit (MCU), wireless transmitting module based on the Bluetooth low energy (BLE) technology, the signal receiver (a smart phone), and the as-fabricated SMS sensor (Fig. 7b). The resistance signal generated by the SMS sensor is converted into corresponding voltage signal, which then realizes analog/digital (A/D) conversion via SP circuits, and the data is further analyzed by MCU and transmitted through the Bluetooth module. Finally, the smart phone receives the wireless signal. To confirm the feasibility of wireless sensing system, a smart warning device towards safety protection is designed (Video S2). As shown in Fig. 7d, the real-time initial resistance of the SMS sensor remains around 16 Ω. When the hammer impacts the SMS sensor, the resistance of the sensor increases to 19.8 Ω (Fig. 7e). The real-time resistance changes during the impact are shown in Fig. 7c recorded by the smart phone. By setting a resistance threshold of 19 Ω, the SMS-based wireless sensor system responds to external impact force by sounding an alarm when the sensor is impacted. Thus, the designed intelligent Bluetooth alarm device can respond to the impact force in time, thus make human body keep away from the external harm. Besides, the wireless signal can also be transmitted between different receivers (Fig. 7f), shows significant application of SMS-based Bluetooth sensing system in wireless transmission and data sharing.

3.8. The anti-impact and sensing property of SMS-based array to various external excitations

On behalf of the lightweight and flexibility of SMS sandwich

composite, the as-developed SMS-based pads can be used as a multifunctional wearable intelligent protective device, providing comprehensive safeguarding ability for human beings under various conditions. The self-adhesion property of SSE polymer enables the designed SMS-based pad can be worn comfortable on different human parts, such as chest, arm and leg to protect human body from the harm of electromagnetic radiation and impact force without any additional adhesives (Fig. 8a), which are beneficial for commercial smart wearable systems. More importantly, it can recognize different stress and presents their distribution via corresponding resistance signals. To show the multiple stimuli-sensing property of wearable SMS-based pads, a 3 × 3 sensor array based on SMS is used to identify various external excitations. Fig. 8d shows the typical electrical signal under bending, which is consistent with the actual pressure distribution (Fig. 8c). Similarly, the stress distribution of the 3 × 3 sensor array under hammer beating corresponds to the resistance signal mappings, demonstrating the sensitivity and precision of the sensor array (Fig. 8f-g). Besides, the 3 × 3 sensor array was further employed to explore the force distribution and impact position when the harsh impact was applied on the array by a drop hammer (Fig. 8h). The array unit in the center records the maximum force while other positions did not show force signals (Fig. 8i). This result is consistent with the resistance distribution (Fig. 8j), which states the impact position can be precisely located in the impact process by the corresponding electrical signals. Thus, the flexible SMS-based array is prospective for perceiving the pressure distribution and protecting human beings from impact and electromagnetic radiation.

4. Conclusion

In this work, a novel SMS sandwich composite with multifunctional sensing property, electromagnetic interference shielding ability and safeguarding performance was designed by assembling SSE polymer, non-woven fabric and conductive MXene. The incorporation of middle MXene-decorated non-woven fabric endows SMS sandwich composite excellent electromagnetic interference shielding performance with the maximum SE_T value of 58 dB. Since the mechanical properties of SSE polymer show rate-dependent characteristic, SMS sandwich composite with ideal shear stiffening property can resist external impact and absorb nearly 97% of impact energy which exhibits superior safeguarding performance. The nonuniformity of stress distribution in the impact process leads to a large number of fracture and destruction of molecular chains in SSE polymer, which is the main mechanism of energy dissipation. Moreover, SMS-based sensor shows multiple stimulus–response properties which can perceive beating, bending and impacting as well as monitoring different human movements. The designed smart alarm device and intelligent manipulator based on SMS sensor also displays its practical application in wireless transmission and human–machine interaction. The final SMS-based array with anti-impact and sensing property to various external excitations can precisely locate external stimuli distributions. Thus, this smart SMS sandwich composite with double-protection for electromagnetic radiation and external impact will exhibit promising applications in human body monitoring and protection, also provide significant guidance for the development of smart wearable protective equipment.

Declaration of Competing Interest

The authors declare that they have no known competing financial interests or personal relationships that could have appeared to influence the work reported in this paper.

Acknowledgements

Financial supports from the National Natural Science Foundation of China (Grant Nos. 12132016, 11972032, 12072338), the Fundamental Research Funds for the Central Universities (WK2480000007), the Joint Fund of USTC-National Synchrotron Radiation Laboratory (KY2090000055), the Anhui's Key R&D Program of China (202104a05020009) and China Postdoctoral Science Foundation (Grant No. 2021M703086) are gratefully acknowledged.

Appendix A. Supplementary data

Supplementary data to this article can be found online at https://doi.org/10.1016/j.cej.2022.135869.

References

[1] B. Peng, F. Zhao, J. Ping, Y. Ying, Recent advances in nanomaterial-enabled wearable sensors: material synthesis, sensor design, and personal health monitoring, Small 16 (2020) 2002681.
[2] R. Yin, D. Wang, S. Zhao, Z. Lou, G. Shen, Wearable sensors-enabled human-machine interaction systems: from design to application, Adv. Funct. Mater. 31 (11) (2021) 2008936.
[3] G. Maddirala, T. Searle, X. Wang, G. Alici, V. Sencadas, Multifunctional skin-compliant wearable sensors for monitoring human condition applications, Appl. Mater. Today 26 (2022), 101361.
[4] R. Stam, S. Yamaguchi-sekino, Occupational exposure to electromagnetic fields from medical sources, Ind. Health 56 (2) (2018) 96–105.
[5] R.D. Carpenter, Human disease resulting from exposure to electromagnetic fields, Environ. Health 28 (2013) 159–172.
[6] W. Chen, L.-X. Liu, H.-B. Zhang, Z.-Z. Yu, Kirigami-inspired highly stretchable, conductive, and hierarchical Ti_3C_2Tx MXene films for efficient electromagnetic interference shielding and pressure sensing, ACS Nano 15 (4) (2021) 7668–7681.
[7] J. Liu, Z. Liu, H.-B. Zhang, W. Chen, Z. Zhao, Q.-W. Wang, Z.-Z. Yu, Ultrastrong and highly conductive MXene-based films for high-performance electromagnetic interference shielding, Adv. Electron. Mater. 6 (2020) 1901094.
[8] W. Chen, L.-X. Liu, H.-B. Zhang, Z.-Z. Yu, Flexible, transparent, and conductive Ti_3C_2Tx MXene-silver nanowire films with smart acoustic sensitivity for high-performance electromagnetic interference shielding, ACS Nano 14 (12) (2020) 16643–16653.
[9] J.-Q. Luo, S. Zhao, H.-B. Zhang, Z. Deng, L. Li, Z.-Z. Yu, Flexible, stretchable and electrically conductive MXene/natural rubber nanocomposite films for efficient electromagnetic interference shielding, Compos. Sci. Technol. 182 (2019), 107754.
[10] L.-X. Liu, W. Chen, H.-B. Zhang, Q.-W. Wang, F. Guan, Z.-Z. Yu, Flexible and multifunctional silk textiles with biomimetic leaf-like MXene/silver nanowire nanostructures for electromagnetic interference shielding, humidity monitoring, and self-derived hydrophobicity, Adv. Funct. Mater. 29 (2019) 1905197.
[11] Y. Zhao, L. Hao, X. Zhang, S. Tan, H. Li, J. Zheng, G. Ji, A novel strategy in electromagnetic wave absorbing and shielding materials design: multi-responsive field effect, Small Sci. 2 (2022) 2100077.
[12] G. Wang, L. Hao, X. Zhang, S. Tan, M. Zhou, W. Gu, G. Ji, Flexible and transparent silver nanowires/biopolymer film for high-efficient electromagnetic interference shielding, J. Colloid Interf. Sci. 607 (2022) 89–99.
[13] Z. Zhang, G. Wang, W. Gu, Y. Zhao, S. Tang, G. Ji, A breathable and flexible fiber cloth based on cellulose/polyaniline cellular membrane for microwave shielding and absorbing applications, J. Colloid Interf. Sci. 605 (2022) 193–203.
[14] M. Zhou, J. Wang, Y. Zhao, G. Wang, W. Gu, G. Ji, Hierarchically porous wood-derived carbon scaffold embedded phase change materials for integrated thermal energy management, electromagnetic interference shielding and multifunctional application, Carbon 183 (2021) 515–524.
[15] G. Wang, S.J.H. Ong, Y. Zhao, Z.J. Xu, G. Ji, Integrated multifunctional macrostructures for electromagnetic wave absorption and shielding, J. Mater. Chem. A 8 (46) (2020) 24368–24387.
[16] Y. Shen, Z. Lin, X. Liu, T. Zhao, P. Zhu, X. Zeng, Y. Hu, R. Sun, C.-P. Wong, Robust and flexible silver-embedded elastomeric polymer/carbon black foams with outstanding electromagnetic interference shielding performance, Compos. Sci. Technol. 213 (2021), 108942.
[17] Y.-J. Wan, X.-Y. Wang, X.-M. Li, S.-Y. Liao, Z.-Q. Lin, Y.-G. Hu, T. Zhao, X.-L. Zeng, C.-H. Li, S.-H. Yu, P.-L. Zhu, R. Sun, C.-P. Wong, Ultrathin densified carbon nanotube film with "metal-like" conductivity, superior mechanical strength, and ultrahigh electromagnetic interference shielding effectiveness, ACS Nano 14 (10) (2020) 14134–14145.
[18] L. Wang, Y. Wu, Y. Wang, H. Li, N. Jiang, K. Niu, Laterally compressed graphene foam/acrylonitrile butadiene styrene composites for electromagnetic interference shielding, Compos. Part A 133 (2020), 105887.
[19] S. Huang, L. Wang, Y. Li, C. Liang, J. Zhang, Novel Ti_3C_2Tx MXene/epoxy intumescent fire-retardant coatings for ancient wooden architectures, J. Appl. Polym. Sci. 138 (2021), e50649.
[20] L. Wang, Z. Ma, Y. Zhang, H. Qiu, K. Ruan, Mechanically strong and folding-endurance Ti_3C_2Tx MXene/PBO nanofiber films for efficient electromagnetic interference shielding and thermal management, Carbon Energy (2022) 1–11.
[21] P. Song, B. Liu, H. Qiu, X. Shi, D. Cao, J. Gu, MXenes for polymer matrix electromagnetic interference shielding composites: A review, Compos. Commun. 24 (2021) 100653.

[22] T.-B. Ma, H. Ma, K.-P. Ruan, X.-T. Shi, H. Qiu, S.-Y. Gao, J.-W. Gu, Thermally conductive poly(lactic acid) composites with superior electromagnetic shielding performances via 3D printing technology, Chinese J. Polym. Sci. 40 (2022) 248.
[23] Y. Zhang, Z. Ma, K. Ruan, J. Gu, Flexible Ti_3C_2Tx/(aramid nanofiber/PVA) composite films for superior electromagnetic interference shielding, Research 2022 (2022) 9780290.
[24] Q.-N. Zhao, Y.-J. Zhang, Z.-H. Duan, S. Wang, C. Liu, Y.-D. Jiang, H.-L. Tai, A review on Ti_3C_2Tx-based nanomaterials: synthesis and applications in gas and humidity sensors, Rare Met. 40 (2021) 1459–1476.
[25] L.-Y. Xiu, Z.-Y. Wang, J.-S. Qiu, General synthesis of MXene by green etching chemistry of fluoride-free Lewis acidic melts, Rare Met. 39 (11) (2020) 1237–1238.
[26] F. Shahzad, M. Alhabeb, C.B. Hatter, B. Anasori, S.M. Hong, C.M. Koo, Y. Gogotsi, Electromagnetic interference shielding with 2D transition metal carbides (MXenes), Science 353 (2016) 6304.
[27] S. Gürgen, M.C. Kushan, W. Li, Shear thickening fluids in protective applications: a review, Prog. Polym. Sci. 75 (2017) 48–72.
[28] H. Zong, Z. Liu, R. Wei, B. Dong, X. Yang, W. Zhai, Shear thickening and impact resistance properties of STG in flexible protection application, J. Phys. 1855 (2021), 012022.
[29] E.E. Haro, A.G. Odeshi, J.A. Szpunar, The energy absorption behavior of hybrid composite laminates containing nano-fillers under ballistic impact, Int. J. Impact Eng. 96 (2016) 11–22.
[30] A. Katiyar, T. Nandi, N.E. Prasad, Impact behavior of aminosilane functionalized nanosilica based shear thickening fluid impregnated Kevlar fabrics, J. Appl. Polym. Sci. 138 (2021) 50862.
[31] C.S. Boland, U. Khan, G. Ryan, S. Barwich, R. Charifou, A. Harvey, C. Backes, Z. Li, M.S. Ferreira, M.E. Möbius, R.J. Young, J.N. Coleman, Sensitive electromechanical sensors using viscoelastic graphene-polymer nanocomposites, Science 354 (6317) (2016) 1257–1260.
[32] S. Wang, S. Liu, J. Zhou, F. Li, J. Li, X. Cao, Z. Li, J. Zhang, B. Li, Y. Wang, X. Gong, Advanced triboelectric nanogenerator with multi-mode energy harvesting and anti-impact properties for smart glove and wearable e-textile, Nano Energy 78 (2020), 105291.
[33] C. Zhao, Y. Wang, S. Cao, S. Xuan, W. Jiang, X. Gong, Conductive shear thickening gel/Kevlar wearable fabrics: A flexible body armor with mechano-electric coupling ballistic performance, Compos. Sci. Technol. 182 (2019), 107782.
[34] S. Wang, L. Ding, X. Fan, W. Jiang, X. Gong, A liquid metal-based triboelectric nanogenerator as stretchable electronics for safeguarding and self-powered mechanosensing, Nano Energy 53 (2018) 863–870.
[35] P. Qu, C. Lv, Y. Qi, L.u. Bai, J. Zheng, A highly stretchable, self-healing elastomer with rate sensing capability based on a dynamic dual network, ACS Appl. Mater. Interfaces 13 (7) (2021) 9043–9052.
[36] S. Wang, L. Gong, Z. Shang, L. Ding, G. Yin, W. Jiang, X. Gong, S. Xuan, Novel safeguarding tactile e-skins for monitoring human motion based on SST/PDMS-AgNW-PET hybrid structures, Adv. Funct. Mater. 28 (2018) 1707538.
[37] C. Yang, A. Abodurexiti, X. Maimaitiyiming, Flexible humidity and pressure sensors realized by molding and inkjet printing processes with sandwich structure, Macromol. Mater. Eng. 305 (8) (2020) 2000287.
[38] C. Xu, Y. Wang, J. Wu, S. Song, S. Cao, S. Xuan, W. Jiang, X. Gong, Anti-impact response of Kevlar sandwich structure with silly putty core, Compos. Sci. Technol. 153 (2017) 168–177.
[39] Y. Guo, H. Qiu, K. Ruan, S. Wang, Y. Zhang, J. Gu, Flexible and insulating silicone rubber composites with sandwich structure for thermal management and electromagnetic interference shielding, Compos. Sci. Technol. 219 (2022), 109253.
[40] Y. Zhang, K. Ruan, J. Gu, Flexible sandwich-structured electromagnetic interference shielding nanocomposite films with excellent thermal conductivities, Small 17 (2021) 2101951.
[41] F. Tarlochan, Sandwich structures for energy absorption applications: A review, Materials 14 (16) (2021) 4731.
[42] M. Tang, P. Zheng, K. Wang, Y. Qin, Y. Jiang, Y. Cheng, Z. Li, L. Wu, Autonomous self-healing, self-adhesive, highly conductive composites based on a silver-filled polyborosiloxane/polydimethylsiloxane double-network elastomer, J. Mater. Chem. A 7 (48) (2019) 27278–27288.
[43] Q.i. Wu, H. Xiong, Y. Peng, Y.i. Yang, J. Kang, G. Huang, X. Ren, J. Wu, Highly stretchable and self-healing "solid-liquid" elastomer with strain-rate sensing capability, ACS Appl. Mater. Interfaces 11 (21) (2019) 19534–19540.
[44] Y. Cheng, X. Li, Y. Qin, Y. Fang, G. Liu, Z. Wang, J. Matz, P. Dong, J. Shen, M. Ye, Hierarchically porous polyimide/Ti_3C_2Tx film with stable electromagnetic interference shielding after resisting harsh conditions, Sci. Adv. 7 (2021) eabj1663.
[45] Y. Zhang, W. Tian, L. Liu, W. Cheng, W. Wang, K.M. Liew, B. Wang, Y. Hu, Eco-friendly flame retardant and electromagnetic interference shielding cotton fabrics with multi-layered coatings, Chem. Eng. J. 372 (2019) 1077–1099.
[46] B. Yao, X. Xu, H. Li, Z. Han, J. Hao, G. Yang, Z. Xie, Y. Chen, W. Liu, Q. Wang, H. Wang, Soft liquid-metal/elastomer foam with compression-adjustable thermal conductivity and electromagnetic interference shielding, Chem. Eng. J. 410 (2021), 128288.
[47] Y. Hu, P. Tang, L. Li, J. Yang, X. Jian, Y. Bin, High absorption shielding material of poly(phthalazinone etherketone)/multiwall carbon nanotube composite films with sandwich configurations, RSC Adv. 9 (2019) 18758.
[48] Y. Fei, M. Liang, Y. Chen, H. Zou, Sandwich-like magnetic graphene papers prepared with MOF derived Fe_3O_4-C for absorption-dominated electromagnetic interference shielding, Ind. Eng. Chem. Res. 59 (1) (2020) 154–165.
[49] Q. Xie, Z. Yan, S. Wang, Y. Wang, L. Mei, F. Qin, R. Jiang, Transparent, flexible, and stable polyethersulfone/copper-nanowires/polyethylene terephthalate sandwichstructured films for high-performance electromagnetic interference shielding, Adv. Eng. Mater. 23 (2021) 2100283.
[50] M. Hu, J. Gao, Y. Dong, K. Li, G. Shan, S. Yang, R.-Y. Li, Flexible transparent PES/silver nanowires/PET sandwich-structured film for high-efficiency electromagnetic interference shielding, Langmuir 28 (18) (2012) 7101–7106.
[51] X. Zhu, A. Guo, Z. Yan, F. Qin, J. Xu, Y. Ji, C. Kan, PET/Ag NW/PMMA transparent electromagnetic interference shielding films with high stability and flexibility, Nanoscale 13 (17) (2021) 8067–8076.
[52] Y. Wang, X. Gong, S. Xuan, Study of low-velocity impact response of sandwich panels with shear-thickening gel cores, Smart Mater. Struct. 27 (2018), 065008.
[53] Y. Cao, Y. Guo, Z. Chen, W. Yang, K. Li, X. He, J. Li, Highly sensitive self-powered pressure and strain sensor based on crumpled MXene film for wireless human motion detection, Nano Energy 92 (2022), 106689.
[54] Z. Yan, L. Wang, Y. Xia, R. Qiu, W. Liu, M. Wu, Y. Zhu, S. Zhu, C. Jia, M. Zhu, R. Cao, Z. Li, X. Wang, Flexible high-resolution triboelectric sensor array based on patterned laser-induced graphene for self-powered real-time tactile sensing, Adv. Funct. Mater. 31 (2021) 2100709.
[55] M. Chao, L. He, M. Gong, N.a. Li, X. Li, L. Peng, F. Shi, L. Zhang, P. Wan, Breathable Ti_3C_2Tx MXene/protein nanocomposites for ultrasensitive medical pressure sensor with degradability in solvents, ACS Nano 15 (6) (2021) 9746–9758.